Sensors and Materials, Vol. 38, No. 4 (2026) 2255–2269
MYU Tokyo

S & M 4435

Thermomechanical Coupling Analysis and Process Window Optimization for Ultrahigh-strength 22MnB5 Steel in Hot Stamping: Simulation Study Using Sensor Data

Jiayi Lu,[1] Qian Chen,[2*] Zhi Li,[3] Wenhui Sun,[4] and Tian-Syung Lan[5]

[1,2]School of Digital Art and Design, Sichuan Technology and Business University, Chengdu, Sichuan 611745, China
[3]Academic Affairs Department, Sichuan Technology and Business University, Chengdu, Sichuan 611745, China
[4]School of Information Science and Engineering, Weifang University of Science and Technology, Weifang 262700, Shandong, China
[5]Department of Information Management, Yu Da University of Science and Technology, 168 Xuefu Rd, Zaoqiao 361, Miaoli, Taiwan

(Received February 4, 2026; accepted April 14, 2026)

Keywords: sheet hot stamping, temperature and stress field, simulation

We investigated the thermomechanical coupling and stress–strain distribution of ultrahigh-strength 22MnB5 steel during hot stamping using a non-isothermal simulation method that accounts for dynamic heat generation from plastic work (Taylor–Quinney effect) and friction. Simulation results of the Livermore Software Technology Corporation–Dynamic Nonlinear Analysis revealed that increasing the stamping speed from 30 to 200 mm/s elevated the minimum sheet temperature from 389.8 to 621.3 °C, reducing the maximum stress from 383 to 152 MPa through thermal softening. At a constant speed of 100 mm/s, raising the initial forming temperature from 700 to 900 °C lowered stress from 262 to 155 MPa but enhanced thinning to 1.527 mm, approaching the 25% limit. Quenching analysis results showed an average cooling rate of 60 °C/s, exceeding the critical 25 °C/s, with the final temperature of 262 °C—below the martensite completion point of 280 °C—ensuring full transformation. Beyond materials processing, the developed method predicts internal stress and temperature gradients that physical sensors cannot capture in closed dies. The results provide calibration data for infrared thermography, acoustic emission sensors, and embedded strain gauges, enabling real-time monitoring and adaptive control in industrial hot stamping. This soft-sensing concept of the developed method complements hard-sensor metrology, advancing intelligent manufacturing. Challenges, including sensor durability under rapid thermal cycles and the integration of virtual and physical sensor feedback loops, can be addressed using the simulation method developed in this study for predictive quality assurance.

1. Introduction

Hot stamping is an essential critical non-isothermal forming process that combines mechanical deformation with rapid cooling to achieve high strength in sheet metals. Being

*Corresponding author: e-mail: chenqianwork2019@163.com
https://doi.org/10.18494/SAM6275

ISSN 0914-4935 © MYU K.K.

different from cold stamping, hot stamping involves complex thermomechanical interactions, including heat transfer, plastic deformation, and phase transformation. Although often described as quasi-static, the process inherently couples thermal, mechanical, and fluid dynamic phenomena. The accurate modeling of these interactions is essential for defining boundary conditions and constructing robust numerical simulations that reflect industrial reality.

The automotive industry's pursuit of lightweight structures that do not compromise passenger safety has accelerated the adoption of ultrahigh-strength steel (UHSS). Among which, boron-alloyed steels such as 22MnB5 are widely used in safety-critical components, including bumper beams, door reinforcements, and crash structures. However, traditional simulations that are designed for the cold stamping of low-carbon steels are inadequate for the hot forming of UHSS. The traditional models assume isothermal conditions and neglect the substantial temperature increase caused by plastic work and friction. According to thermodynamic principles, a significant fraction of plastic work is converted into heat, a phenomenon known as the Taylor–Quinney effect.[1] In addition, intense tool–sheet contact generates frictional heating. Therefore, when ignoring these self-heating mechanisms, stamping forces, localized thinning, and springback are inaccurately predicted or estimated.[2,3] To overcome such limitations of traditional simulation methods, thermomechanically coupled simulations are required to capture the dynamic evolution of stress and temperature fields. By identifying temperature thresholds for deformation resistance, thermal processing windows are optimized for advanced dual-phase boron steels. The thresholds obtained can be used for the calibration of high-temperature sensors used in hot stamping presses.

Infrared cameras, thermocouples, and embedded stress sensors rely on the accurate modeling of heat generation and dissipation to interpret signals correctly. Therefore, we simulated the temperature and stress fields of UHSS in hot stamping to align numerical predictions with industrial practice. The results enhance understanding of how temperature fluctuations affect rheological behavior and microstructural evolution while simultaneously advancing the development of sensor-based monitoring strategies. By establishing a simulation framework that functions as a virtual sensor, a gap between computational modeling and physical sensing can be filled, providing a basis for intelligent manufacturing systems to enable predictive process control and quality assurance. The simulation method developed in this study can be applied to materials processing, the results of which contribute to the advancement of sensor-assisted manufacturing, where sensing concepts are integrated to monitor and control thermomechanical coupling in real time.

2. Literature Review

In the stamping process, the conversion of mechanical force to heat through friction and plastic deformation increases the temperature of the workpiece, creating a thermal gradient.[4] Low-carbon steels show high plasticity and low internal stress, which result in negligible temperature increases. However, the widespread use of UHSS has introduced new challenges. Because of its high yield strength, UHSS presents significant stress changes during deformation, accumulating considerable plastic strain energy within the metal lattice.[4] This leads to self-

heating effects, where the temperature increase is ten times greater than that of conventional steels, necessitating a thermomechanically coupled analysis.

Researchers have mainly focused on external heating methods in warm and hot stamping for UHSS and magnesium-aluminum alloys. However, the spontaneous heating of DP steels remains under-researched. Cai *et al.* established a temperature-related yield criterion for DP590 (the tensile strength level of up to 590 Mpa) through warm tensile tests,[5] while Sung *et al.* utilized the Hollomon–Voce model to compare the temperature-dependent properties of DP590, DP780, and DP980.[6] The effect of temperature on rheological stress is prominent in materials such as 22MnB5.[7]

22MnB5 is a boron-alloyed steel that is widely used in vehicles for hot stamping applications. It presents high strength, ductility, and hardenability, which are essential for safety-related parts, including bumper beams, door reinforcements, and structural parts. UHSS with 22MnB5 is a specialized manganese-boron alloy containing 0.22% C, 1.2% Mn, and 0.002% B, and is mainly used in the automotive industry to provide high-performance crash resistance while reducing vehicle weight. During hot stamping, the material is heated to an austenitic state (>900 °C) and then quenched within the die to form a martensitic structure.[3] This process requires extreme precision in thermal monitoring, as even minor temperature deviations can lead to localized failures.

To observe temperature increases in parts made of UHSS, high-speed cameras and infrared monitors are used.[8] However, the method lacks a temperature-dependent stress component, necessitating a sophisticated simulation of their coupling effect. The simulation of a large-scale deformation caused by a temperature-dependent stress is conducted by using an explicit finite element solver, the Livermore Software Technology Corporation–Dynamic Nonlinear Analysis (LS-DYNA), which is well known for highly nonlinear, transient dynamic finite element analysis. LS-DYNA is designed to adopt time integration and the dynamic response of inelastic structures under high-speed impact or explosion. It is regarded as the global standard for simulating complex stamping processes.

Its ability to handle nonlinearity makes it ideal to simulate the hot stamping of UHSS. LS-DYNA is well suited to the analysis of the dynamics because it provides robust thermomechanical coupling. This allows the simulation to function as a virtual sensor by calculating variables that are difficult to measure physically, such as internal stress and instantaneous temperature changes caused by plastic work, in microseconds during a stamping stroke.[9] Its capability is critical for developing intelligent sensing frameworks where simulation data guide real-time process adjustments.

In sheet metals, an increase in temperature promotes material softening and increases the kinetic energy of metal atoms, reducing deformation resistance and enhancing plasticity. Conversely, at higher strains exceeding 0.1, the dislocation density increases, leading to material hardening. At this stage, the strain rate becomes the dominant factor affecting the material's resistance. An essential parameter in studying coupling behavior is the Taylor–Quinney coefficient (TQC), defined as the ratio of generated heat to plastic work.[10] In its instantaneous form, this coefficient is also referred to as the inelastic heat fraction (IHF). Autila *et al.* observed that high-strength steel specimens experience a temperature increase by more than 38 °C upon

fracture.[11] Since deformation energy is not entirely converted to heat, a conversion factor must be input into numerical models.[12] To accurately measure TQC, uniaxial tensile tests must be conducted on slender rods under defined thermal boundary conditions. In the test, one-dimensional heat conduction models are widely used to account for all major thermal effects.[13] Perez-Castellanos and Rusinek employed the Zehnder model in finite element simulations to estimate heat conversion during dynamic compression.[14]

In the era of Industry 4.0, monitoring hot stamping processes for 22MnB5 steel has evolved toward intelligent metrology and sensor-driven manufacturing. Conventional sensing methods, such as infrared thermography, are constrained by optical obstruction during die closure, while thermocouples provide only discrete, point-based measurements that fail to capture full-field thermal gradients.[15] These limitations lead to a growing demand for soft sensors, computational models to identify and estimate process variables from measurable parameters, and provide continuous, spatially resolved data streams.[16]

3. Methodology

3.1 Material

We selected the hot-rolled steel 22MnB5 produced by Baosteel, China, as the stamping material. The mechanical properties of 22MnB5 are listed in Table 1,[4] and its continuous cooling transformation (CCT) curve is shown in Fig. 1.[17] This steel exhibits an Ac_3 temperature of 811°C, the temperature at which the transformation to austenite is complete, and an Ac_1

Table 1
Specifications and mechanical properties of 22MNB5.

Thickness (mm)	Vickers hardness	Yield strength	Tensile strength	Elongation
2	193	485 MPa	666 MPa	19%

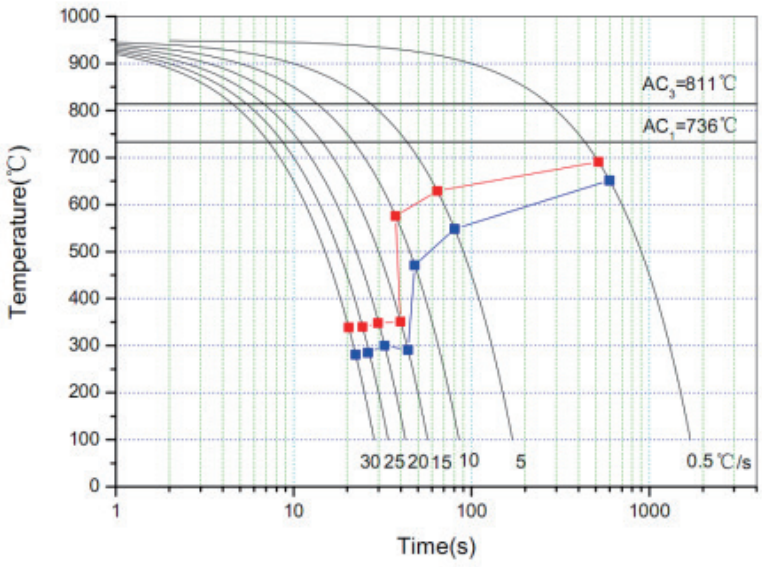

Fig. 1. (Color online) CCT diagram of 22MNB5.

temperature of 736 °C, the temperature at which austenite begins to form during heating. The critical cooling rate is approximately 15 °C/s, with martensite transformation starting between 350 and 380 °C and completing between 280 and 300 °C. A_{c1} is the lower boundary of the intercritical zone. The values of A_{c1} and A_{c3} are used to define the operational limits of the virtual thermal sensor. To ensure the full martensitic transformation required for a tensile strength of 1500 MPa, the real-time monitoring system must verify that the blank temperature exceeds A_{c3} before the quenching phase begins.[18] Predicting the spatial distribution of these temperatures across the blank allows for the identification of under-heated zones that physical sensors might miss, ensuring uniform material properties through sensor-informed simulation.

Figure 2 shows the stress–strain curves of 22MnB5 at different temperatures under a cooling rate of 70 °C/s and a strain rate of 0.01 s^{-1}.[3] The increasing temperature reduces the material's resistance to deformation, while the increasing strain enhances the resistance owing to strain hardening resulting from the high density of dislocations. At large strains of greater than 0.1, the effect of strain magnitude on stress becomes negligible, and the strain rate becomes the dominant factor affecting deformation resistance. This indicates the importance of temperature in determining the rheological stress of 22MnB5. As temperature increases, atomic mobility increases, leading to material softening, reduced resistance to deformation, and enhanced plasticity. Hot stamping technology exploits this principle to form UHSS.

The elastic modulus and yield strength are critical parameters affecting the stamping quality of 22MnB5. Although often assumed to be constant in engineering practice, the elastic modulus and yield strength vary with temperature and plastic deformation. As shown in Fig. 3, changes are minimal below 200 °C. Above this threshold temperature, both parameters decrease rapidly. Such a reduction enables the hot stamping of UHSS. At the same time, Poisson's ratio remains stable, between 0.31 and 0.33, in the temperature range of 600–900 °C.[3]

When the temperature exceeds 800 °C, the yield strength and elastic modulus stop decreasing and stabilize. Consequently, the hot forming of steel at temperatures above 800 °C requires lower stamping forces, improves sheet flowability, and enhances stamping (Fig. 4).[19] Figure 4

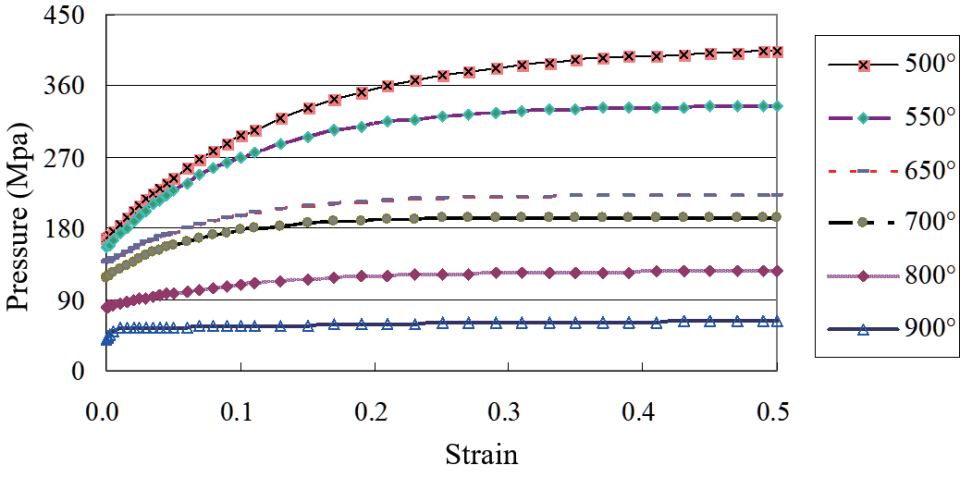

Fig. 2. (Color online) Stress–strain curves of 22MnB5 at different temperatures.

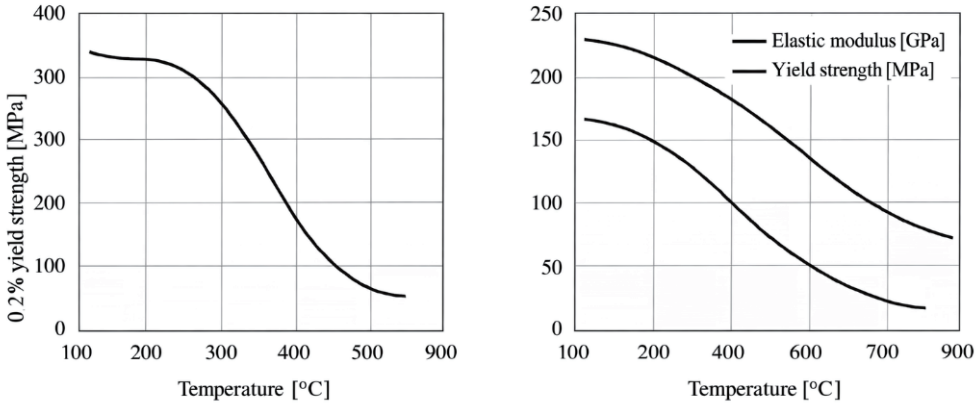

Fig. 3. Variation of yield strength and elastic modulus with temperature of 22MnB5.

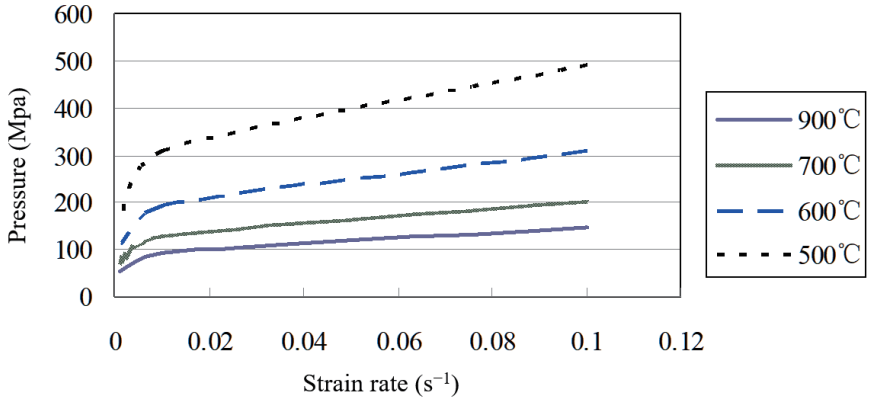

Fig. 4. (Color online) Combined effect of strain rate and temperature on deformation resistance of 22MnB5.

shows the combined effect of strain rate and temperature on deformation resistance at a strain of 0.1. Under identical temperature conditions, deformation resistance increases with strain rate. In stamping processes, excessive forming speed must be avoided to prevent stress concentration and fracture. Between 700 and 900 °C, the effect of strain rate on deformation resistance is smaller than between 500 and 700 °C. For example, at a strain rate of 0.1 s^{-1}, deformation resistance values are approximately 500 MPa at 500 °C, 200 MPa at 700 °C, and 150 MPa at 900 °C (Fig. 4). Therefore, the initial forming temperature needs to be set above 700 °C to minimize deformation resistance, reduce fracture risk, and lower the required press capacity.

3.2 Simulation method

For hot stamping simulations, 22MnB5 was modeled using LS-DYNA with Belytschko–Tsay shell elements. The Hill48 yield criterion with isotropic hardening was applied to capture anisotropic behavior. The Hill48 yield criterion is a mathematical model developed by Rodney Hill in 1948 to describe the plastic yielding of anisotropic materials, particularly sheet metals. While common yield criteria assume that a material behaves the same in all directions (isotropy),

Hill48 accounts for the fact that metals have different yield strengths in the rolling, transverse, and thickness directions as a result of the manufacturing process. To reduce computational cost, only half of a car door impact beam was analyzed, exploiting geometric symmetry. The bumper beam dimensions (1071 × 100.81 × 35.4 mm) were discretized into a finite element mesh (Fig. 5). This digital twin serves as a virtual sensor, generating continuous maps of stress and temperature fields that can be compared with die-embedded thermocouples and strain gauges.

Then, the Norton–Hoff law was used to describe thermoviscous behavior, with parameters calibrated from Gleeble 3800 experiments. Instead of presenting full derivations, the model is summarized as follows. The thermoviscous behavior of 22MnB5 is characterized, where the flow stress (σ) is expressed as a function of strain (ε), strain rate ($\dot{\varepsilon}$), and temperature (T). This mathematical equation is the core of the virtual sensor, enabling the prediction of internal stress states by integrating real-time inputs of deformation speed and thermal gradients. The parameters, including the hardening exponent of 0.31, were calibrated using empirical data from Gleeble 3800 sensors, ensuring that the digital twin accurately reflects the physical material's response.

$$\sigma = 50.12\varepsilon^{0.31}\dot{\varepsilon}^{0.07}\exp\left(\frac{2542}{T}\right) \tag{1}$$

Here, stress depends on strain, strain rate, and temperature. This equation is used for calibrating data for soft sensors, enabling the prediction of thermal and mechanical responses that physical sensors cannot measure directly inside closed dies.

3.2.1 Hot stamping

Industrial hot stamping begins with austenitization at 900–950 °C, followed by transfer to the press. Simulations were initialized between 700 and 900 °C with stamping speeds of 20–200 mm/s. At 700 °C, increasing the speed from 30 to 200 mm/s increased the minimum sheet temperature from 389.8 to 621.3 °C while reducing the maximum stress from 383 to 152 MPa. At 100 mm/s, the increasing initial temperature from 700 to 900 °C lowered stress from 262 to 155 MPa, but thinning approached the 25% limit. The optimal processing window was identified as 750–900 °C and 35–100 mm/s, balancing low deformation resistance with acceptable thinning.

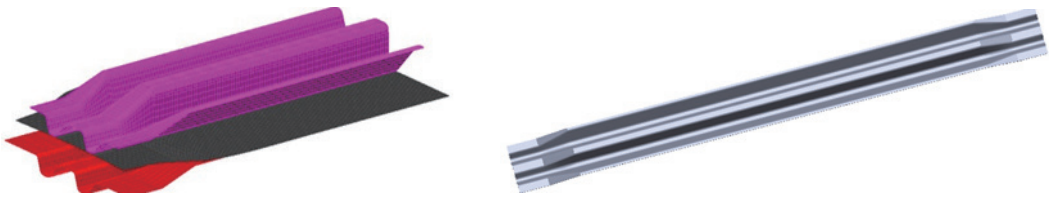

Fig. 5. (Color online) FA mesh model and 3D numerical model of bumper beam.

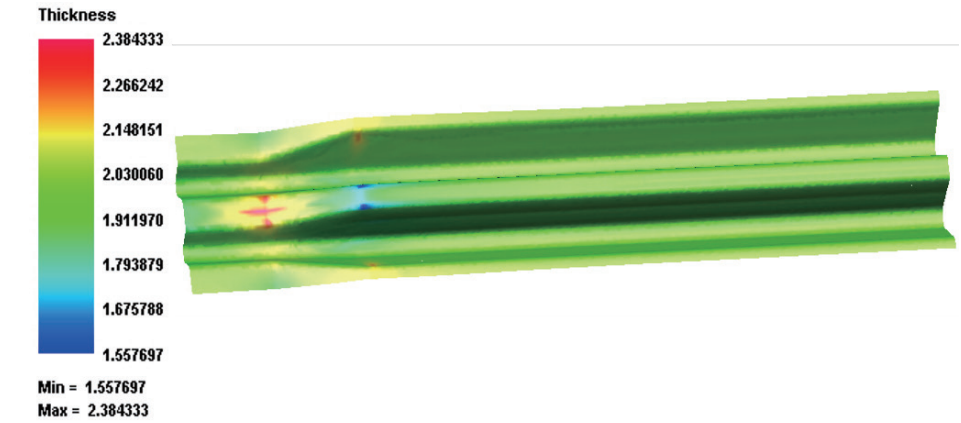

(a)

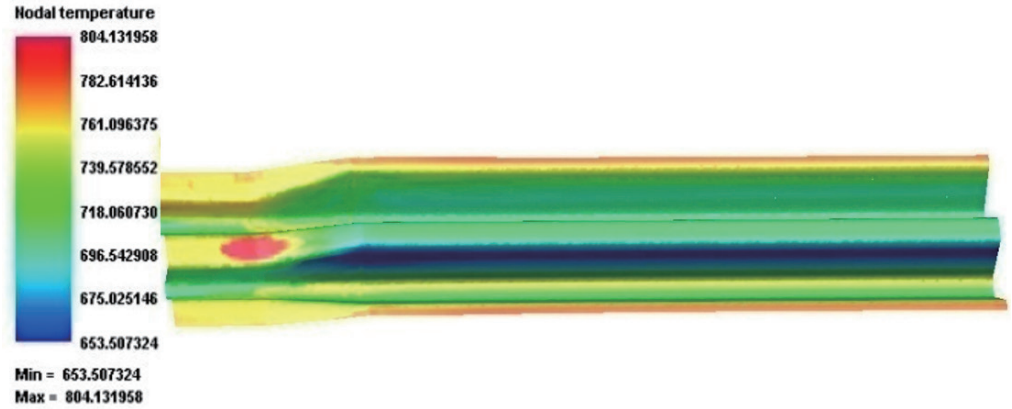

(b)

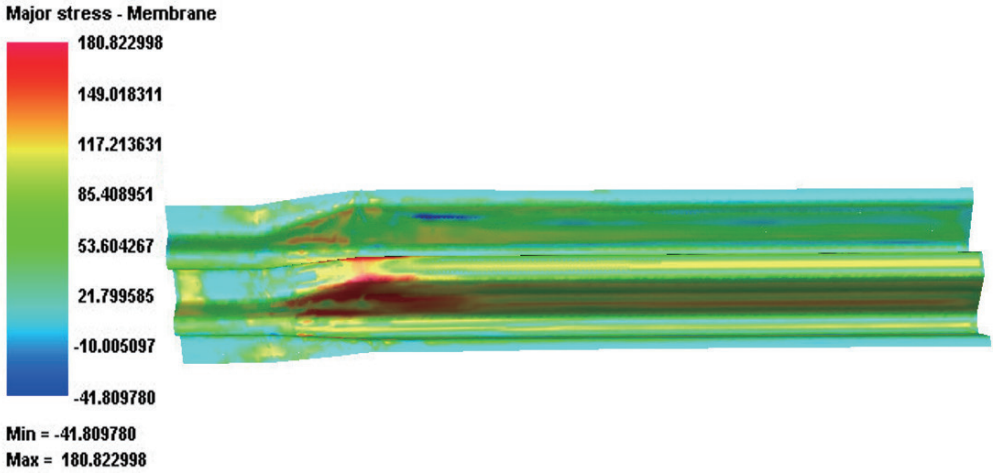

(c)

Fig. 6. (Color online) Cloud maps of simulation results of parameter distributions during hot stamping. (a) Thickness (red cross on left side presents Point A). (b) Temperature (red spot on left side presents Point B). (c) Maximum stress. (d) Maximum strain.

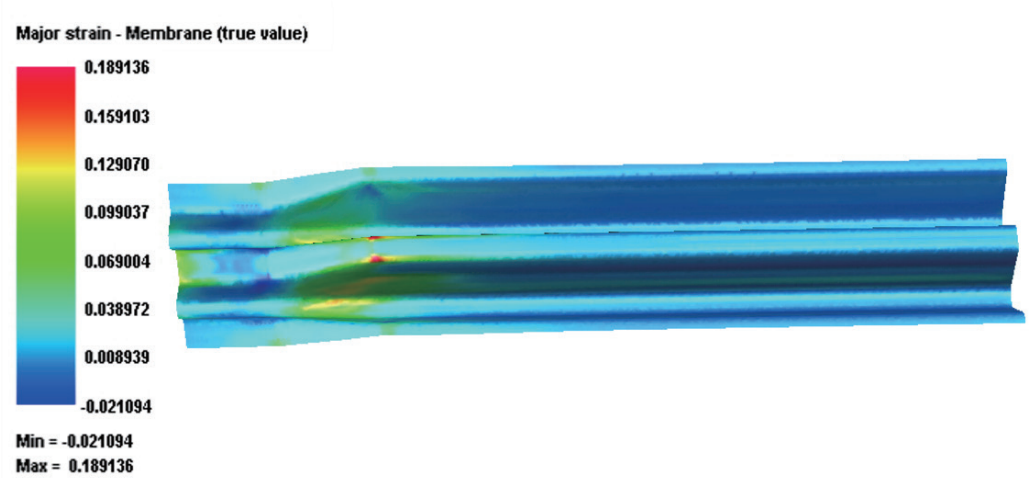

(d)

Fig. 6. (Continued) (Color online) Cloud maps of simulation results of parameter distributions during hot stamping. (a) Thickness (red cross on left side presents Point A). (b) Temperature (red spot on left side presents Point B). (c) Maximum stress. (d) Maximum strain.

Figure 6 illustrates thickness, temperature, stress, and strain distributions. These maps act as virtual sensor outputs, guiding the placement of infrared sensors (for thermal monitoring) and acoustic emission sensors (for stress localization). For example, Point A (minimum thickness of 1.56 mm) coincides with maximum stress concentration (up to 181 MPa), highlighting a critical region for sensor deployment. Therefore, the simulation results not only define safe operating windows for 22MnB5 but also provide actionable data for sensor calibration and smart die design, ensuring that physical sensors capture the most critical thermal and mechanical events during stamping.

3.2.2 Temperature and stress in quenching

Quenching is the final stage of hot stamping and ensures martensitic transformation and dimensional stability. In our simulation, a specimen formed at 900 °C and 100 mm/s was quenched for 10 s under pressure. The cooling profile (Table 2) showed an average rate of 60 °C/s, exceeding the 25 °C/s required for full martensitic transformation. Cooling was nonlinear: reaching 90 °C/s in the first second, decreasing to 30 °C/s by the fifth second. After 10 s, the maximum temperature reached 262 °C, which is below the martensite completion threshold of 280 °C, confirming complete transformation.

The results can be used as calibration data for thermocouples and infrared monitoring systems. Data from thermocouples embedded in dies can be validated against the predicted cooling curve, while infrared sensors can be used to detect localized heat retention. Figure 7 illustrates the temperature distribution, highlighting extruded regions that retained higher temperatures owing to poor die contact. These areas represent critical zones where physical

Table 2
Temperature range during 10 s of holding after quenching.

Quenching time (s)	0	1	2	3	4	5	6	7	8	9	10
Maximum temperature (°C)	855	764	683	615	553	491	437	385	340	299	262
Lowest temperature (°C)	692	605	517	442	378	322	271	234	198	172	148

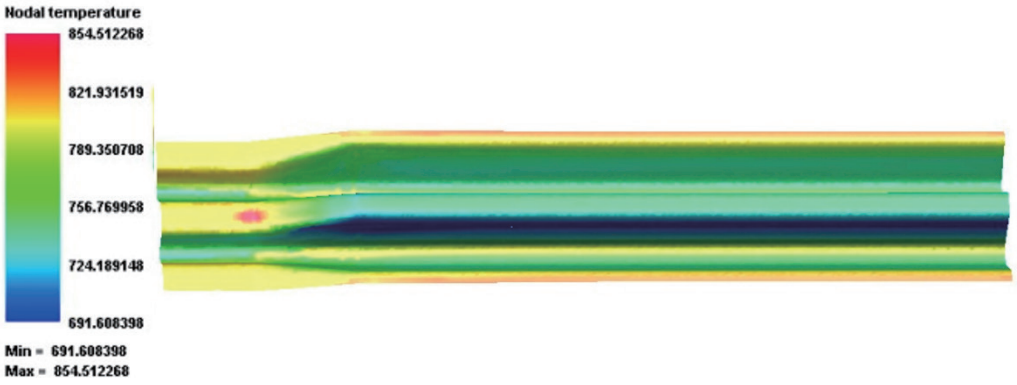

(a)

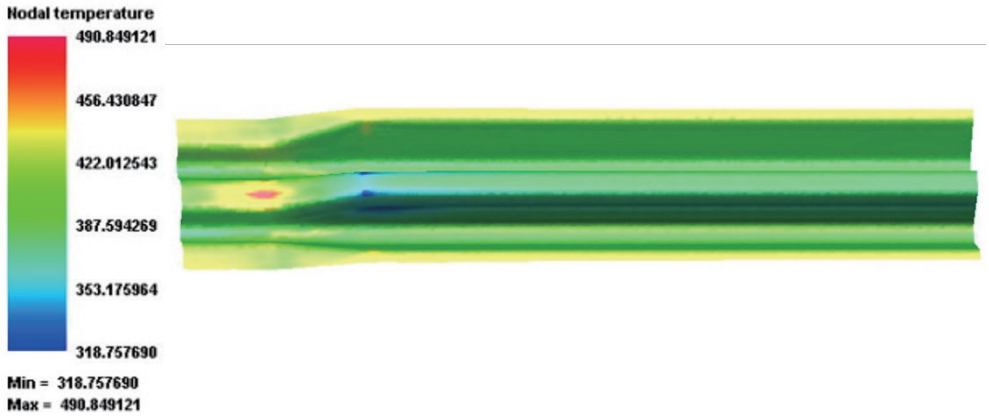

(b)

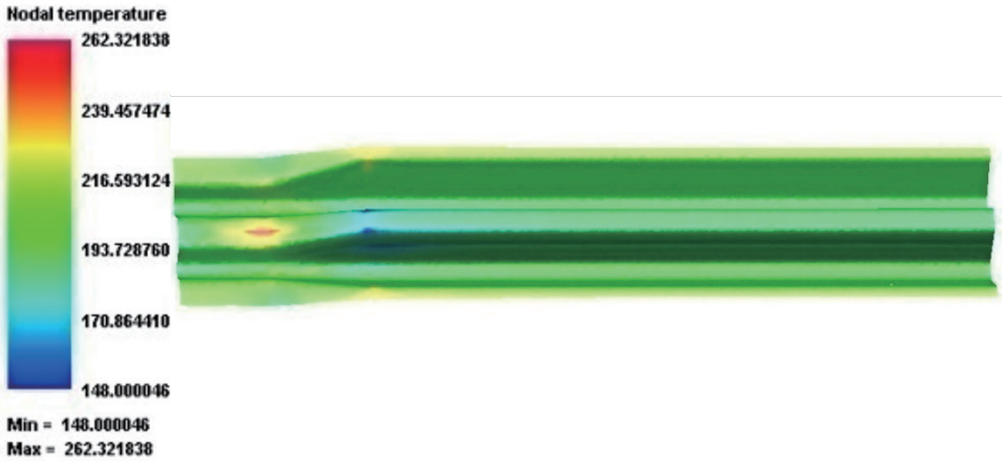

(c)

Fig. 7. (Color online) Cloud maps of temperature during quenching. (a) Thickness. (b) Temperature. (c) Maximum stress.

sensors may underperform, underscoring the need for virtual sensing models to complement hard-sensor data.

Thickness distributions before and after quenching (Figs. 8–10) showed a high uniformity of 90% for the thickness of 2 mm. This smoothing effect validates the role of sensor-assisted dimensional monitoring, ensuring quality control in industrial practice. Therefore, the quenching simulations not only confirm metallurgical transformation but also establish a framework for sensor calibration, placement, and validation, bridging computational predictions with real-time monitoring in smart stamping lines.

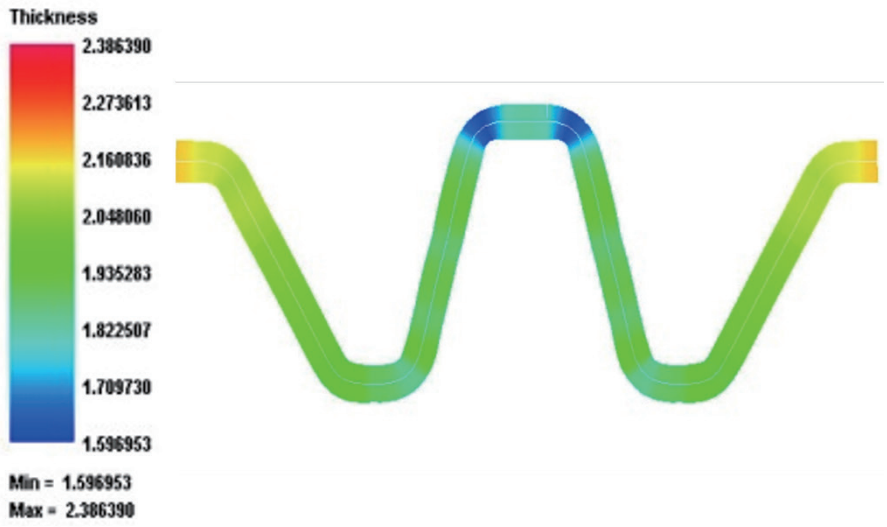

Fig. 8. (Color online) Thickness distribution of sections before quenching.

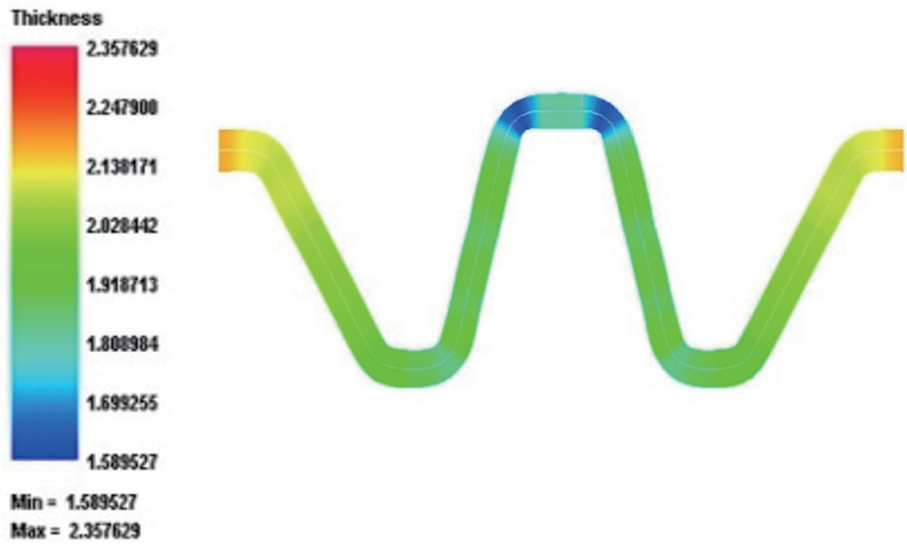

Fig. 9. (Color online) Thickness distribution of sections after quenching.

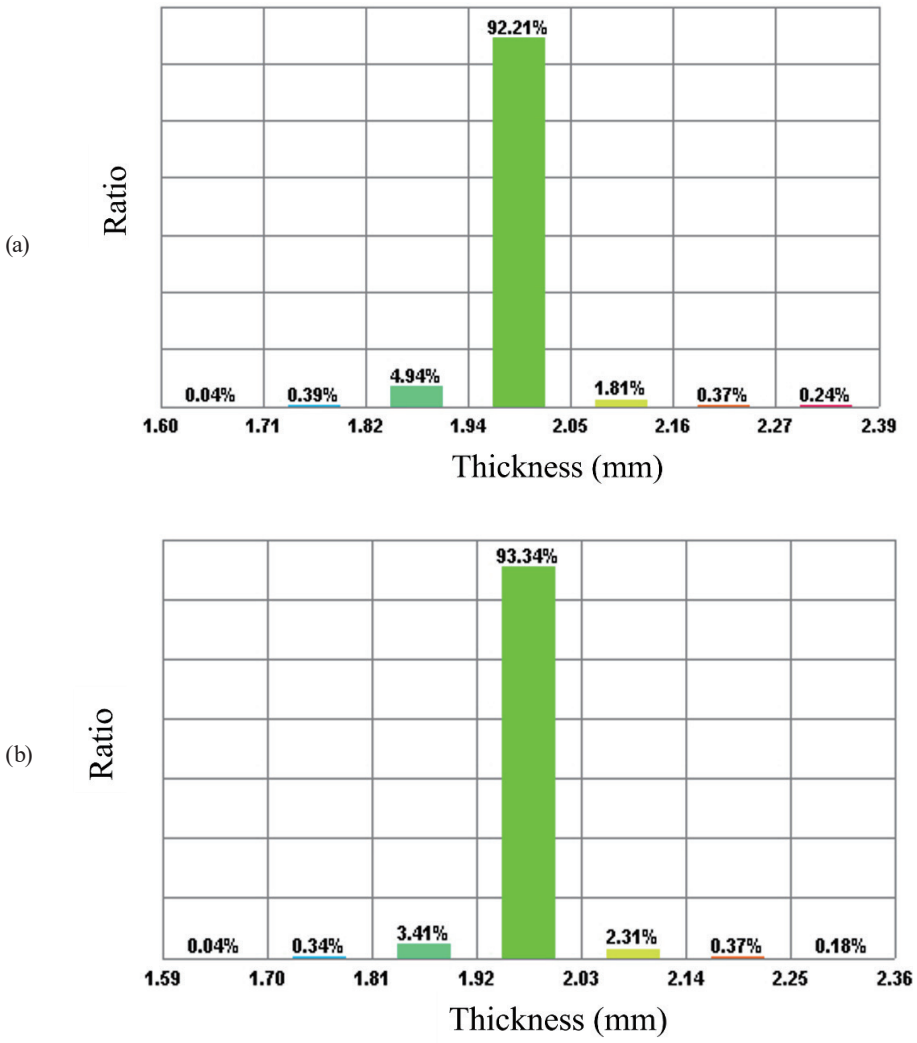

Fig. 10. (Color online) Thickness distribution ratios of sheet metal (a) before and (b) after quenching.

4. Discussion

The simulation results in this study can be used to identify an operational window for the hot stamping of 22MnB5. On the basis of the results in Tables 3 and 4, the optimal processing conditions are defined as an initial temperature between 750 and 900 °C and a stamping speed of 35–100 mm/s. Within this range, deformation resistance is minimized, thinning remains below the 25% threshold, and the sheet temperature stays above the martensite initiation point of 380–400 °C. These findings are consistent with experimental results on hot stamping. Merklein and Lechler demonstrated through industrial trials that in the hot stamping of 22MnB5, forming and quenching can be successfully combined in one step, producing crash-relevant automotive components with high strength and minimal springback.[3] More recently, Wróbel *et al.* have reported an experimental evaluation of hot-stamped 22MnB5 autobody parts, confirming that simulation predictions of stress and thinning trends align with measured sensor data.[2]

Table 3
Simulation results at initial stamping temperature of 700 °C.

Stamping speed (mm/s)	Minimum thickness (mm)	Minimum temperature (°C)	Maximum stress (MPa)	Maximum strain
30	1.721	389.8	383	0.128
35	1.706	426.2	346	0.133
50	1.691	475.3	291	0.135
100	1.657	530.2	262	0.141
150	1.628	577.6	173	0.209
200	1.584	621.3	152	0.315

Table 4
Simulation data for stamping speed of 100 mm/s.

Initial forming temperature (°C)	Minimum thickness (mm)	Minimum temperature (°C)	Maximum stress (MPa)	Maximum strain
700	1.657	530.2	262	0.141
750	1.637	573.6	233	0.153
800	1.591	615.3	210	0.171
850	1.557	653.5	181	0.189
900	1.527	691.6	155	0.237

Other than materials processing, the simulation results offer a reference for sensor deployment in industrial hot stamping lines. Infrared sensors can be strategically positioned to ensure that sheet temperatures remain above martensite initiation thresholds, while acoustic emission sensors can detect stress concentrations at thinning sites. For example, the region of maximum thinning coincides with the highest stress concentration (181 MPa), making it the best location for acoustic monitoring. Similarly, infrared cameras can be used to track thermal gradients across the sheet, ensuring uniform cooling and preventing localized defects.

The predicted cooling rates during quenching (60 °C/s average, with initial peaks near 90 °C/s) align with the values measured using thermocouples in Gleeble experiments, validating the simulation as a virtual sensing system. The simulation result provides a high-resolution map of temperature and stress fields throughout the stamping cycle, functioning as a soft sensor that complements physical measurements. Such virtual sensing enables the optimization of smart dies, identifying regions of elevated wear or critical thermal thresholds where die-embedded sensors should be placed. By integrating predictive modeling with sensor deployment, manufacturers can conduct adaptive process control, predictive maintenance, and automated quality assurance. By using the results of the simulation, hard-sensor metrology and computational soft sensing can be complemented for improved integrated, sensor-assisted hot stamping in Industry 4.0.

5. Conclusions

A thermomechanical coupling method was developed to simulate the hot stamping of UHSS as a virtual sensor to overcome the physical limitations of in-die metrology. The results revealed that stamping speed and initial temperature are synergistic determinants of formability.

Increasing the stamping speed from 30 to 200 mm/s resulted in a significant 60% reduction in flow stress, driven by enhanced thermal retention and adiabatic heating. To ensure structural integrity, an optimal process window was identified at initial temperatures higher than 750 °C and speeds higher than 35 mm/s, maintaining the blank above the 380–400 °C threshold throughout deformation and limiting maximum thinning to 20%. The quenching phase, utilizing a 10 s pressure-holding duration, achieved an average cooling rate of 90 °C/s. This significantly exceeds the critical 27–30 °C/s threshold required for 22MnB5, ensuring a complete martensitic transformation below the 280 °C martensite finish temperature. Furthermore, thickness uniformity was optimized, with 90% of the component stabilizing at the 2.0 mm nominal value.

By offering validated thermal and stress profiles, the developed simulation method provides the calibration data necessary for the deployment of physical sensors, such as infrared thermography, acoustic emission sensors, and die-embedded thermocouples, in extreme manufacturing environments. This integration supports the transition to smart dies capable of real-time, closed-loop control and predictive maintenance. Despite these advancements, pending problems remain, including the limited durability of physical sensors under rapid thermal cycles, the high computational cost of real-time virtual sensing, and the need for high-resolution data fusion to capture localized stress concentrations. It is necessary to validate the virtual sensing model against multi-axial stress sensors in industrial-scale tooling to strengthen the reliability of sensor-driven, intelligent manufacturing systems.

References

1 G. I. Taylor and H. Quinney: Proc. R. Soc. London, Ser. A **143** (1934) 307. https://www.jstor.org/stable/96095
2 I. Wróbel, A. Skowronek, and A. Grajcar: Symmetry **14** (2022) 969. https://doi.org/10.3390/sym14050969
3 M. Merklein and J. Lechler: J. Mater. Process. Technol. **177** (2006) 452. https://doi.org/10.1016/j.jmatprotec.2006.03.233
4 M. Naderi, L. Durrenberger, A. Molinari, and W. Bleck: Mater. Sci. Eng., A **478** (2008) 130. https://doi.org/10.1016/j.msea.2007.05.094
5 Z. Cai, M. Wan, Z. Liu, X. Wu, B. Ma, and C. Cheng: Int. J. Mech. Sci. **126** (2017) 79. https://doi.org/10.1016/j.ijmecsci.2017.03.009
6 J. H. Sung, J. H. Kim, and R. H. Wagoner: Int. J. Plast. **26** (2010) 1746. https://doi.org/10.1016/j.ijplas.2010.02.005
7 Metal Zenith: https://metalzenith.com/blogs/steel-properties/22mnb5-steel-properties-and-key-applications?utm_source=copilot.com (accessed January 2026).
8 J. Choi, B. Choi, S. Heo, Y. Oh, and S. Shin: Appl. Therm. Eng. **128** (2018) 159. https://doi.org/10.1016/j.applthermaleng.2017.09.001
9 J. Martschin, M. Wrobel, J. Grodotzki, T. Meurer, and A. E. Tekkaya: Automot. Innovation **6** (2023) 352. https://doi.org/10.1007/s42154-023-00238-z
10 X. Qiao, F. Cao, M. Su, C. Yang, T. Li, G. Ding, Y. Tan, Y. Chen, H. Wang, M. Jiang, and L. Dai: J. Appl. Phys. **135** (2024) 145103. https://doi.org/10.1063/5.0191314
11 M. Autila, E. Lantto, and A. Arkkio: IEEE Trans. Magn. **34** (1998) 684. https://doi.org/10.1109/20.668066
12 M. B. Jabłońska: Arch. Civ. Mech. Eng **23** (2023) 135. https://doi.org/10.1007/s43452-023-00656-00
13 P. Knysh and Y. P. Korkolis: Mech. Mater. **86** (2015) 71. https://doi.org/10.1016/j.mechmat.2015.03.006
14 J.-L. Perez-Castellanos and A. Rusinek: J. Theor. Appl. Mech. **50** (2012) 377. https://www.researchgate.net/publication/282990107
15 K. J. Tilly, E. Scharifi, and D. Bailly: MATEC Web Conf. **408** (2025) 01050. https://doi.org/10.1051/matecconf/202540801050
16 H.-S. Choi, B.-M. Kim, D.-H. Kim, and D.-C. Ko: Int. J. Precis. Eng. Manuf. **15** (2104) 1087. https://doi.org/10.1007/s12541-014-0441-7

17 J. Brnic, M. Brcic, S. Krscanski, J. Niu, S. Chen, and Z. Gao: Metals **10** (2020) 1445. https://doi.org/10.3390/met10111445
18 H. Karbasian and A. Tekkaya: J. Mater. Process. Technol. **210** (2010) 2103. https://doi.org/10.1016/j.jmatprotec.2010.07.019
19 W. He, B. Yang, X. Zhang, M. Li, S. Sun, B. Wang, and Q. Ma: Metals **14** (2024) 561. https://doi.org/10.3390/met14050561